Fire performance of charring closed-cell polymeric insulation materials: polyisocyanurate and phenolic foam

Fire performance of charring closed-cell polymeric insulation materials: polyisocyanurate and phenolic foam

Juan P. Hidalgo[a,b1], José L. Torero[b], Stephen Welch[a]

[a] School of Engineering, The University of Edinburgh, Edinburgh, EH9 3JL, UK

[b] School of Civil Engineering, The University of Queensland, Brisbane St Lucia, QLD 4072, Australia

Abstract

Results are presented from two series of ad-hoc experimental programmes using the Cone Calorimeter to investigate the burning behaviour of charring closed-cell polymeric insulation materials, specifically polyisocyanurate (PIR) and phenolic (PF) foams. These insulation materials are widely used in the construction industry due to their relatively low thermal conductivity. However, they are combustible in nature; therefore, their fire performance needs to be carefully studied, and characterisation of their thermal degradation and burning behaviour is required in support of performance-based approaches for fire safety design. The first series of experiments was used to examine the flaming and smouldering of the char from PIR and PF. The peak heat release rate per unit area was within the range of 120 to 170 $kW \cdot m^{-2}$ for PIR and 80 to 140 $kW \cdot m^{-2}$ for PF. The effective heat of combustion during flaming was within the range of 13 to 16 $kJ \cdot g^{-1}$ for PIR and around 16 $kJ \cdot g^{-1}$ for PF, while the CO/CO_2 ratio was within 0.05 to 0.10 for PIR and 0.025 to 0.05 for PF. The second experimental programme served to map the thermal degradation processes of pyrolysis and oxidation in relation to temperature measurements within the solid-phase under constant levels of nominal irradiation. Both programmes showed that surface regression due to smouldering was more significant for PF than PIR under the same heat exposure conditions, essentially because of the different degree of overlap in pyrolysis and oxidation reactions. The smouldering of the char was found to self-extinguish after removal of the external heat source.

Keywords

Insulation materials; Charring foams; Pyrolysis; Smouldering; Combustion; Performance-based design

Nomenclature

$E_{CO \rightarrow CO_2}$	heat release per mass unit of oxygen consumed for the combustion of carbon monoxide ($J \cdot g^{-1}$)

[1] Corresponding author: j.hidalgo@uq.edu.au

E_{O_2}	heat release per mass unit of oxygen consumed ($J \cdot g^{-1}$)
ΔH_c	heat of combustion ($J \cdot g^{-1}$)
m	mass ($g \cdot s^{-1}$)
$\overline{m}$	normalised mass (-)
$\dot{m}$	mass flow rate ($g \cdot s^{-1}$)
$\dot{Q}$	heat release rate (W)
t	time (s)
T	temperature (K or °C)
X	volume fraction ($mol \cdot mol^{-1}$)
$\dot{V}$	volumetric flow ($m^3 \cdot s^{-1}$)

Greek letters

γ	volumetric expansion factor (-)
ϕ	oxygen depletion factor (-)

Subscripts

0	Initial
air	of air
eff	Effective
end	of the end duration of the test
e	of the exhaust or extraction
i	of the species i
$loss$	of total loss from the sample
s	loss from the sample

Acronyms

CDG	carbon dioxide generation calorimetry
DTG	differential thermogravimetric analysis
HRR	heat release rate
HRRPUA	heat release rate per unit area
OC	oxygen consumption calorimetry
PIR	closed-cell rigid polyisocyanurate foam
PF	closed-cell rigid phenolic foam
TC	Thermocouple
TGA	thermogravimetric analysis

1. Introduction

Stringent requirements for energy efficiency are driving a trend towards the more widespread use of insulation materials in the built environment. Several types of insulation materials, which are able to meet

the multiple design criteria often required for buildings, can be found in the market. A typical classification for insulation materials in the European market, proposed by *Papadopoulos et al.* [1], distinguishes four main groups: (1) inorganic materials such as foams or fibrous materials, (2) organic materials such as expanded foams or fibrous materials, (3) combined materials, and (4) new technology materials. Expanded organic foams such as closed-cell rigid polyisocyanurate (PIR) and phenolic foam (PF) are common combustible insulation materials that are increasingly being used for the design of energy-efficient buildings due to their relatively low thermal conductivity, low density, good durability and ease of installation [2]. These factors, in conjunction with the requirement for lower thermal transmittances in building assemblies [3], lead to these materials increasingly being a preferred option for design.

1.1. Fire hazards from combustible insulation

The increase in production and extended usage of combustible materials in buildings such as closed-cell cellular polymers has recently given rise to several concerns in the fire safety community [4, 5]. This is however not a new problem, and many aspects have already been addressed by several authors and institutions in the past [6]. Indeed, in order to identify the potential fire hazards to life safety from insulation materials in buildings, numerous authors have extensively studied the fire performance of different types of insulation under different approaches [6-24]. The biggest concern, represented as the flammability and energy release, has classically been addressed using bench-scale experimentation [13-22], e.g. determining the Limiting Oxygen Index (LOI) according to ASTM D2863 [27] and assessing ignition properties, heat release and flame spread by using the Cone Calorimeter [28] or the LIFT apparatus [29]. During recent decades, the fire performance of these materials has been improved by applying flame retardancy techniques, i.e. promoting charring behaviour and endothermic reactions in the solid phase, which is typically researched at material scale using thermogravimetry [7-9]. The generation of toxic species due to the combustion and pyrolysis of these plastics has also been raised as a potentially significant concern, and several authors have studied the toxicity of emissions from insulation materials commonly used in buildings [10-12].

While most of this work has clearly served to rate the hazard from insulation products under specific testing scenarios, several authors highlight that the extrapolation of the performance observed from small-scale testing is hardly applicable to larger scale due to the combination of complex phenomena [23-26]. Although significant efforts are constantly made to reduce the flammability/combustibility of these materials, there is potential for confusion from the belief that the risk associated with these hazards can be effectively mitigated by obtaining better ratings from standard testing. Harmonisation of standardised testing is intended to offer a plausible representation of the fire hazards from construction products. Yet,

quantification of the risks associated with the use combustible insulation in buildings remains as a significant challenge for practitioners.

1.2. Design tools to quantify the risk from combustible insulation

Recently, new methodologies for the fire safe design of insulation systems have been proposed based on their material behaviour under severe conditions of heat exposure [30]. The methodology proposed by *Hidalgo et al.* (2015) considers the mitigation of the fire hazard from combustible insulation materials by designing suitable thermal barriers that control the onset of pyrolysis [30, 31], i.e. delaying the onset of hazard generation. Previous work demonstrated that the onset of hazard could be conservatively defined as a 'critical temperature' [32]. For charring foams, the 'critical temperature' was defined as the temperature at which the peak of the main pyrolysis reaction is obtained by differential thermogravimetric analyses (DTG) at sufficiently low heating rates and under non-oxidative atmospheres.

The proposed methodology represents a conservative approach for the quantitative fire safe design of construction systems including insulation materials; i.e. a framework by which the risk can be quantified. Nevertheless, additional models are required by practitioners and regulatory bodies if quantification of the evolution of hazard after the onset of pyrolysis is to be understood [33], i.e. potential heat release contribution and generation of toxic species from the insulation. The quantification of these hazards is determined by the terms (1) production rate of pyrolysis gases, (2) heat of combustion from pyrolysis gases and (3) gas species generated by the pyrolysis and combustion. In order to be able to quantify these parameters and propose a model for performance-based design, a thorough understanding of the material behaviour under conditions of heat exposure is required. This study aims at achieving a thorough understanding of the material behaviour beyond standard testing and parameters, thus identifying the underlying processes that govern those issues, i.e. the thermal degradation and thermal evolution of the condensed phase at a relevant scale.

1.3. Research significance and objectives

In previous work, we presented studies on flammability properties from PIR and PF, as well as their thermal decomposition processes at a material scale by thermogravimetry [32]. The purpose of that work was to determine parameters for the proposed performance-based design methodology [30]. Values of 'critical temperature' established previously, which represent the onset of hazard (pyrolysis), correspond to 300 – 370 °C for rigid PIR insulation and 425 °C for the specific phenolic foam studied [32]. The present work explores the fire performance of these materials based on their burning behaviour. Variables such as the heat of combustion, emissions of carbon monoxide (CO) and carbon dioxide (CO_2) and consumption of oxygen (O_2) from the combustion are assessed. Thus, the information presented here aims to provide

relevant data for the development and application of models capable of predicting the production rate of energy, pyrolysis, and combustion products under different scenarios.

Then, the scope of the work presented herein is to present an original methodology to assess the fire performance of representative samples of two common commercial rigid closed-cell plastic insulation materials (polyisocyanurate and phenolic foam). This work explores which phenomena should be considered for the development and application of models that can quantify their burning hazard. In order to achieve this, the following goals are pursued:

- Macroscopic analysis of the fire performance of these foams by studying heat release rate, mass loss, and gas emissions from Cone Calorimeter ad-hoc experiments.
- Mapping of the thermal degradation processes in relation to temperature measurements within the solid-phase, correlating the evolution of the thermal profile experienced by the material to results obtained by thermogravimetric analyses presented elsewhere [32].

The present work is vital for the further development of engineering tools that could assist performance-based designs of building assemblies including combustible insulation. As noted by *Hidalgo et al.* [30], whereas the current regulatory fire safety frameworks in the EU [34, 35] do not provide a suitable approach for insulation materials, further instrumentation and inclusion of quantitative approaches could complement current standardised testing practices. This approach would help to provide a better understanding and quantification of the fire hazards from insulation materials.

It should be noted that the final fire performance of plastic foams such as PIR and PF strongly depend on the chemical composition and manufacturing process [36]; e.g. content of isocyanurate linkages and type of isocyanate-reactive component for PIR, or degree of reticulation for phenolic foams. This information is however largely inaccessible to the public. Since the purpose of this work is to establish a methodology that allows for a comprehensive analysis of phenomena relevant to the eventual fire performance characterisation, three current commercially available types of PIR from different manufacturers were selected. These products are certified by their manufacturers to correspond to isocyanurate-based foams (PIR) rather than urethane-based foams (PUR). Only one phenolic foam product was selected aiming at a performance comparison with respect to PIR foams; previous thermogravimetric studies have shown essential differences between these products [32].

2. Experimental programme description

The experimental programme designed to achieve the objectives noted above was based on the use of the Cone Calorimeter apparatus [28], as two different series of ad-hoc experiments:

(1) Piloted experiments and transferring the heat to the sample by radiation from the cone, as presented for the flammability experiments on insulation materials presented elsewhere [32]. The main measurements consisted of mass loss and gas species such as oxygen, carbon dioxide and carbon monoxide, supported by visual observations.

(2) Non-piloted experiments and transferring the heat to the sample by radiation from the cone. The main measurements consisted of gas species and temperature measurements within the samples, supported by visual observations.

2.1. Materials

The studied insulation materials comprised three types of rigid polyiscocyanurate foam (hereby referred as PIRa, PIRb and PIRc, respectively) and one type of phenolic foam (PF). These thermoset plastics are manufactured as rigid closed-cell polymers by blowing a gas through the entire structure of the foam. At present, the blowing agents mainly utilised are n-Pentane, iso-Pentane, cyclo-Pentane and various hydrofluorocarbons that have zero ozone depleting potential [37].

Three different PIR foams from various suppliers were selected to assess the difference in their performance. Polyisocyanurate, which is manufactured based on the mix of an organic isocyanate component and an isocyanate-reactive component, is known to present different possible formulations depending on the isocyanate-reactive component used, which determines its thermal stability [8]. Results in further sections show that the characteristic fire performance from the three foams was similar. Therefore, for studying phenolic foam, only one product was selected with the intention to assess its characteristic performance with respect to PIR foam.

These materials are often supplied as rigid boards with a protective layer on the surface, which is expected to have some impact on the observed performance during the tests. For the products studied herein, the protective layer corresponds to a low emissivity composite aluminium foil/paper facing. In order to examine this, samples with and without protective layer were tested. Nevertheless, it should be noted that since this work mainly pursued the characterisation of the material, rather than the product to specific testing methods, the effect of the protective layer must be addressed carefully. Samples with a surface area of 90 mm by 90 mm and 100 mm thick were tested in the two series of experiments. Samples with the protective layer removed are shown in Figure 1.

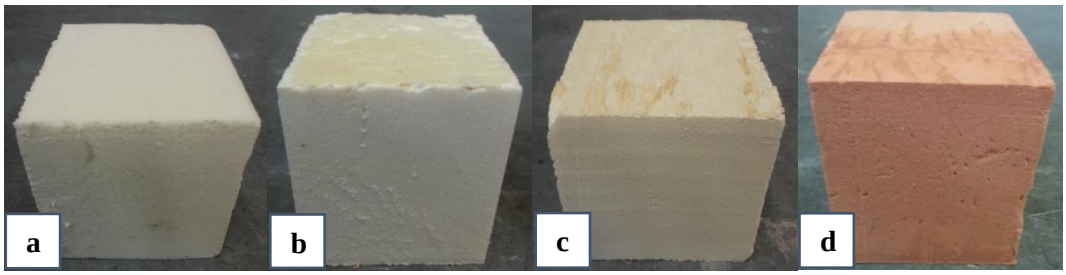

Figure 1. Samples of insulation materials before testing.
(a) PIRa (b) PIRb (c) PIRc (d) PF.

2.2. Set-up #1: Piloted experiments with the heat transferred by radiation

The set-up of these experiments is detailed elsewhere [32], the results of which are complementary to those presented here. In the previous publication, the measurements were used to assess the critical temperature and thermal inertia of several insulation materials for a performance-based methodology. Temperature measurements were not taken for this experimental programme. The results presented in following sections will rather focus on heat release rate, mass loss, heat of combustion and gas emissions. These provide an assessment of the burning behaviour of these foams with no protective layer, thus a characterisation of the material rather than the product.

2.3. Set-up #2: Non-piloted experiments with the heat transferred by radiation

For these experiments, samples were wrapped with aluminium foil at the bottom and lateral sides, with a 6 mm Nickel 200 block at the bottom, and altogether wrapped in two 3 mm thick layers of ceramic insulation paper. The aluminium foil was mainly used to prevent air penetration in the sample from the sides and only allow it from the top. From a heat transfer perspective, the foil is transparent for the conducted heat due to its low thickness and high thermal diffusivity, thus acting as a thermally thin material. The two layers of ceramic paper were used in order to reduce the thermal gradients on the surface of the sample sides. It should be noted that an adiabatic boundary condition at the sides will always be unattainable with this set-up since the conductivity of the ceramic paper is higher than the materials tested[2]. A schematic drawing of the conceptual set-up and the real set-up are shown in Figure 2 and Figure 3, respectively.

[2] Thermal conductivity of ceramic paper: 0.08 and 0.11 $W \cdot m^{-1} \cdot K^{-1}$ at 600 and 800°C, respectively.

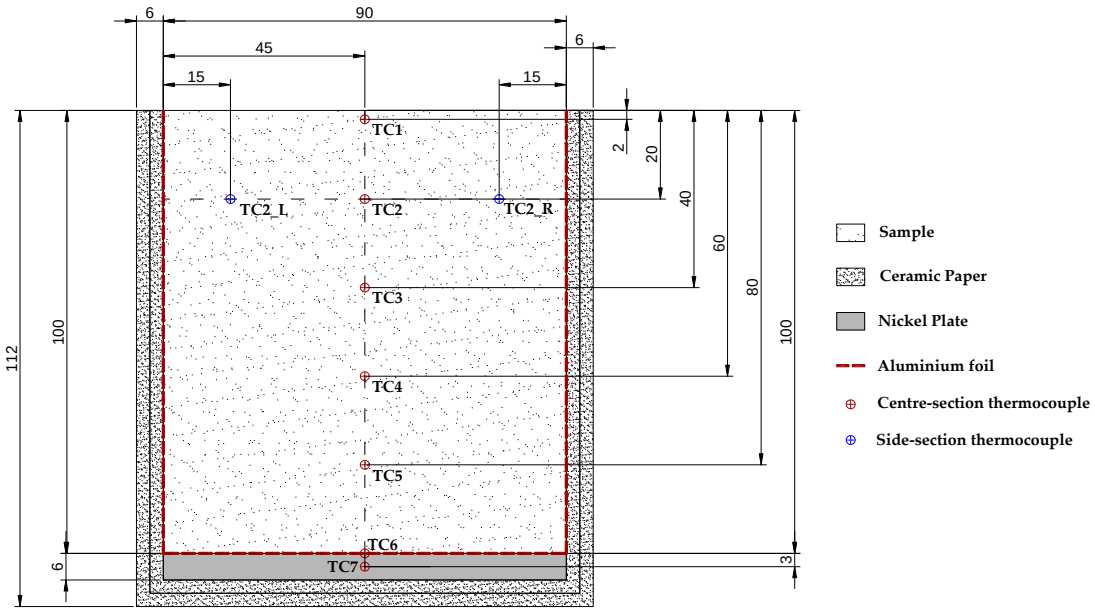

Figure 2. Schematics of sample preparation for the set-up #2.

It should be noted that this set-up was used to provide relevant and reliable results that could facilitate future modelling tasks. Thus, the characterisation of the boundary condition at the back face of the material is achieved by using the 6 mm Nickel 200 plate at the bottom of the samples. This approach was described by *Carvel et al.* [38], who recommended the use of a heat sink for material characterisation purposes.

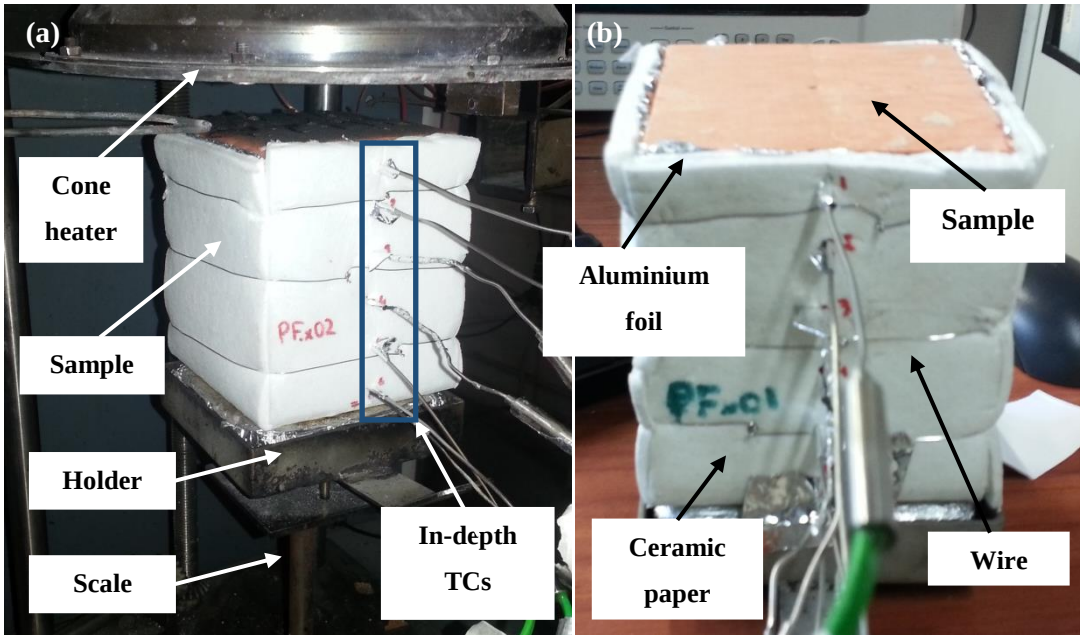

Figure 3. (a) Sample during testing (b) Sample prepared before testing.

As for the boundary condition at the exposed surface, several values of irradiation from the radiant heater were used. The heat fluxes were selected in such a way that mapping of the different thermal

183 degradation processes was highlighted. The minimum heat flux for each material was defined as a thermal
184 exposure that did not trigger the onset of pyrolysis after reaching thermal equilibrium. Specific values of
185 external heat flux for each material are noted in Table 1.

186 Experiments were performed at least twice in order to verify the repeatability of the results, and for
187 two different configurations, i.e. with no protective layer and with a non-coloured protective layer attached
188 to the exposed surface in order to explore different phenomena and thermal behaviour experienced by the
189 foams.

190 Measurements of temperature were taken within the sample by using 1.5 mm bead K-type
191 thermocouples. The temperature of the metallic plate at the back was also measured. Thermocouples were
192 installed at the centre of the section and every 2 mm in-depth and in parallel to the exposed surface with
193 the intention of reducing the error in the thermocouple measurement, which is a recommended procedure
194 for materials of particularly low conductivity [39, 40]. The first thermocouple was placed within a range of
195 2-3 mm from the surface. No temperature correction was considered by the heat losses introduced by the
196 thermocouple. Additionally, two thermocouples were inserted 30 mm horizontally off the second in-depth
197 thermocouple for some experiments. This procedure aimed to clarify whether the heat transfer through the
198 sample was behaving either one-dimensionally or two-dimensionally. The positioning of the thermocouples
199 is shown in Figure 2. A summary of the conditions for all the performed experiments is presented in Table
200 1.

201 Gas species such as carbon dioxide, carbon monoxide and oxygen were measured at the apparatus
202 exhaust duct, which nominal volumetric flow corresponded to 24 $l \cdot s^{-1}$. Mass loss was not measured for this
203 experimental programme, as the thermocouples would interfere with the measurements.

204 Table 1. Summary of performed experiments (set-up #2).

<table>
<tr><th>Material</th><th>Configuration</th><th>Incident radiant heat flux range /kW·m^{-2}</th><th>Measured parameters</th></tr>
<tr><td>PIRa
Manufacturer-claimed density:
31 - 34 kg/m^3
Average measured density:
31.2 ± 0.61 kg/m^3</td><td rowspan="2">Nominal sample size:
90 mm x 90 mm x 100 mm
Exposed surface:
(a) With protective layer
(b) Without protective layer
Wrapping:
2 layers of ceramic paper + 1 layer of aluminium foil
Back boundary condition:
Nickel 200 plate (6 mm) + Ceramic board (25 mm)
Orientation:
Horizontal
Pilot:</td><td>10, 25, 35

(2 repetitions)</td><td rowspan="2">(1) In-depth temperature

(2) O_2, CO_2 and CO gas species</td></tr>
<tr><td>PIRb
Manufacturer-claimed density:
32 kg/m^3
Average measured density:
33.0 ± 0.71 kg/m^3</td><td>5, 10, 25, 35

(2 repetitions)</td></tr>
</table>

PIRc Manufacturer-claimed density: 30 - 32 kg/m^3 Average measured density: 33.5 ± 0.65 kg/m^3	No pilot igniter	5, 10, 25, 35 (2 repetitions)	
PF Manufacturer-claimed density: 35 kg/m^3 Average measured density: 38.1 ± 1.05 kg/m^3		5, 10, 15, 25 (2 repetitions)	

3. Analysis methodology

The calorimetry approach considered to evaluate the heat release rate (HRR) from the burning of the insulation materials is the species evolution approach based on oxygen consumption (OC) [41]. Oxygen consumption rather than carbon dioxide generation calorimetry (CDG) [42] is used to correlate the HRR due to two main reasons: (1) the desiccation system based on calcium sulphate (*drierite*®) tends to absorb carbon dioxide when anhydrous, thus affecting the shape of the measured curve of carbon dioxide, and (2) the variability of energy coefficients for CDG tends to be larger than OC [44]. Then, the formulation considered for the experiments corresponds to OC calorimetry, noted in Eq. (1), which was originally proposed by *Janssens* [43] and has been revisited by *Biteau* [44]:

$$\dot{Q}_{OC} = \left(E_{O_2} \cdot \phi - \left(E_{CO\rightarrow CO_2} - E_{O_2}\right) \cdot \frac{1-\phi}{2} \cdot \frac{X_{CO}}{X_{O2}}\right) \cdot \frac{\dot{m}_{ex}}{1+\phi\cdot(\gamma-1)} \cdot \frac{M_{O_2}}{M_{air}} \cdot X_{O_2}^0 \quad (1)$$

where E_{O_2} and $E_{CO\rightarrow CO_2}$ are the energy released per mass unit of oxygen consumed (W·g^{-1}) and per mass unit of oxygen consumed for the combustion of carbon monoxide respectively (W·g^{-1}), $\dot{m}_e$ is the mass flow in the exhaust (g·s^{-1}), γ is the volumetric expansion factor (-), M_{O_2} and M_{air} are the molecular weight of oxygen and air respectively (g·mol^{-1}), and ϕ is the oxygen depletion factor (-).

The effective heat of combustion $\Delta H_{c,eff}$ (J·g^{-1}) is quantified based on calculations of HRR and experimental mass loss, given by:

$$\Delta H_{c,eff} = \frac{\int_0^{t_{end}} \dot{Q}_{OC}(t)\cdot dt}{m_{loss}} \quad (2)$$

where $\dot{Q}_{OC}(t)$ is the heat release rate (W), t_{end} is the end time of the test (s), and m_{loss} is the total mass loss during the test (g). The notation 'effective' relates to an average value obtained by the combustion of the material. However, the combustion process for most of these foams is non-uniform, with transition from flaming to smouldering, as will be shown in further sections. Then, if Eq. (2) is applied for the total test time, the obtained values of heat of combustion will represent a lumped value that considers both flaming

and smouldering as a single process. The effective heat of combustion from pyrolysis gases for materials that char and experience smouldering is attempted for an arbitrary period up to 200 seconds during the initial flaming combustion. This period is chosen considering the samples exposed to heat fluxes larger than 35 kW.m^{-2} (refer to Figure 5). Even though a shorter integration time would be more adequate for 25 kW.m^{-2}, this would lead to large errors due to the short transient behaviour of the flaming combustion. It should be noted that, whereas this is an arbitrary criterion, the objective is to compare this value to the effective value considering the total time of the test.

Mass measurements from the samples are normalised with respect to the initial mass of the sample, m_0 (g), as shown in Eq. (3) below:

$$\bar{m}(t) = \frac{m(t)}{m_0} \tag{3}$$

where $\bar{m}(t)$ and $m(t)$ are the normalised mass (-) and measured mass (g), respectively, at any time. As discussed in further sections, the ceramic paper used to prepare the samples is expected to lose mass during the test, thus including an overestimation of the mass loss. This error is estimated as a maximum of 5% of the initial sample mass, which is assessed by running tests at high heat fluxes until almost all the sample is consumed.

In order to assess the different thermal degradation processes with respect to temperature measurements, the duration of the tests from experimental set-up #2 was selected in a way such that the maximum thermal gradient could be compared to the residue of the sample. Therefore, samples were cut through their centre-section after the end of the test, and the level of thermal degradation achieved at different depths assessed by visual colourimetry. Additionally, the consistency of these results is correlated with thermogravimetric experiments presented elsewhere [32, 36].

4. Results and Discussion

4.1. Burning behaviour

A summary of the experimental results consisting of mass loss of the samples, heat release rate per unit area (HRRPUA), and gas species correlations for PIRa and PF are presented below. For simplicity, and since the results from the rest of PIR materials are very similar in performance, only results from PIRa are discussed in this section.

4.1.1. General observations

The three types of PIR were found to behave similarly, with a very fast ignition for every external heat flux larger than the critical. This was followed by a small flame which continued to be reduced until

intermittent flaming was only observed by the edges of the sample. Polyisocyanurate foam tended to expand slightly at early stages of the heat exposure. After flaming, a black char layer remained which tended to glow if the external heat flux was high. The char at the surface continued to get consumed by oxidation and its thickness started to reduce at different rates depending on the incident radiant heat flux. Flaming at the edges was sporadically observed. The remaining char from PIR was very soft and light. Discolouration of the PIR samples was observed, changing from yellow to orange-brown and finally black colour during the process of thermal degradation. This discolouration is discussed in further sections. It should be noted that the similarity between results from the three types of PIR foams is extensively discussed in [36]. Therefore, herein only main comparative results are presented, and a greater focus is put on PIRa. The reader is referred to [36] for assessing the differences in behaviour for three different PIR foams.

Phenolic foam was found to have a similar behaviour to PIR, proceeding to char formation after flaming and to smoulder after flame out at the surface. As shown in previous studies [32], the critical heat flux for ignition is larger than PIR (10-15 $kW \cdot m^{-2}$ for PIR, 22 $kW \cdot m^{-2}$ for PF); however, its surface regression by smouldering after ignition was shown here to be much faster. Phenolic foam tended to spall and crack very easily during heat exposure and presented a more brittle behaviour. Popping and snapping sounds could be heard during testing. Discolouration was observed, changing from pink-brown to yellow and finally black colour during the process of thermal degradation. This discolouration is discussed in further sections.

4.1.2. Normalised mass

Figure 4 shows the average curves of normalised mass from two repetitions for PIRa and PF without protective layer at the surface of the samples. For simplicity in the visual assessment of the different evolution of the tests, the mass data is presented as a normalised mass. The normalised mass here refers to the ratio between the mass at any time and the initial mass of the sample before the start of test ($m(t)/m_0$). Therefore, a normalised value of 1 indicates the initial state where the mass of the sample is equal to the initial mass of the sample; a value of 0 indicates that the whole sample has been consumed. For high heat fluxes, samples were tested until near complete consumption of the sample (5% of the mass). Tests at lower heat fluxes (25 – 45 $kW.m^{-2}$ for PIR, 25 $kW.m^{-2}$ for PF) were interrupted earlier, and the sample was removed as no significant flaming was visible anymore. It should be noted that the sample holder materials also experienced loss of mass; therefore, the normalised measurement includes a maximum error or overestimation of up to a 5%. This explains why the curves presented in Figure 4 reach an absolute normalised mass of 0 in some instances. Due to the unknown mass loss evolution of the sample holder, a correction has not been applied as this would include further uncertainty in the data outputs.

The mass loss curves of PIR present a reducing slope throughout the tests, indicating that the pyrolysis front was moving through thickness leaving a protective char, thus decreasing the rate of pyrolysis. However, since smouldering was also experienced at the surface of the sample after charring, the change of slope also includes this phenomenon. Phenolic foam mass loss curves are more linear than the ones observed for PIR, while PF mass loss is also observed to be larger than PIR for the same heating conditions. This behaviour is indicative of a more severe consumption of the char at the surface by oxidation (smouldering) for PF. This is consistent with thermogravimetric experiments presented elsewhere [32], which indicated that while PIR presents its main pyrolysis (250-350 °C) and oxidation (500-650 °C) domains in two different temperature regions, the PF main pyrolysis (400-500 °C) and oxidation (480-550 °C) slightly overlap in the same temperature region.

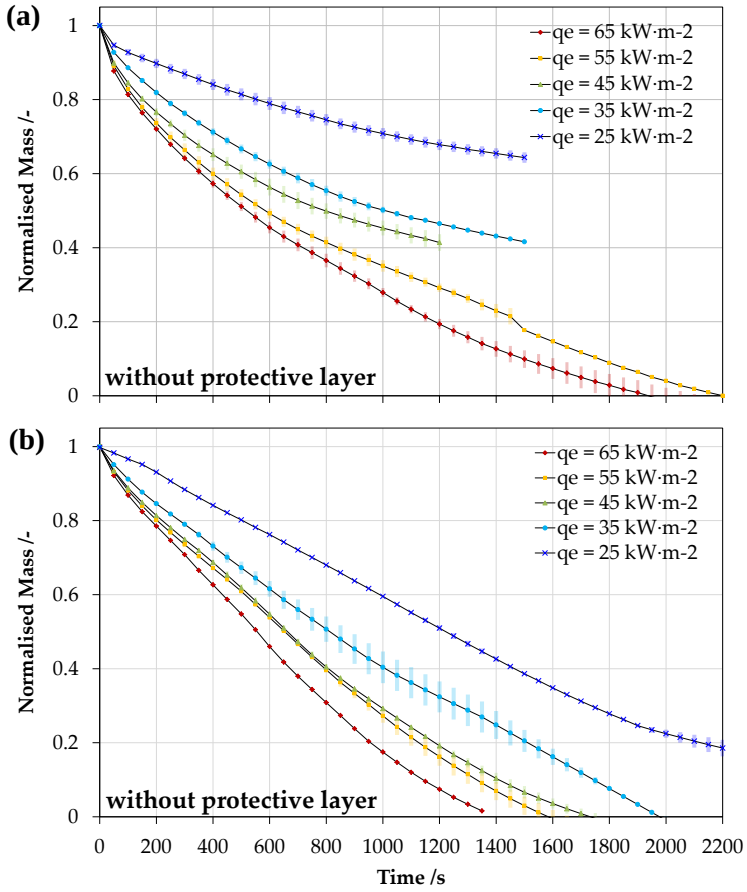

Figure 4. Normalised mass ($m(t)/m_0$) of (a) PIRa and (b) PF samples without protective layer at different heat fluxes. Shading indicates std. dev. from two repetitions.

4.1.3. Heat release rate per unit area and effective heat of combustion

Figure 5 shows the average heat release rate per unit area (HRRPUA) from two repetitions for PIRa and PF. In general, PIR samples showed lower HRRPUA than PF throughout the test, except for the peak

of HRRPUA. The burning behaviour of PIR and PF showed similar trends, with a large peak of HRRPUA right after ignition, followed by a progressive decay, which is characteristic of charring materials. This is generally expected for any PIR. Nevertheless, PF showed a decay of HRRPUA after the first peak, but an increase for high heat fluxes, which reflects a faster consumption of the char layer.

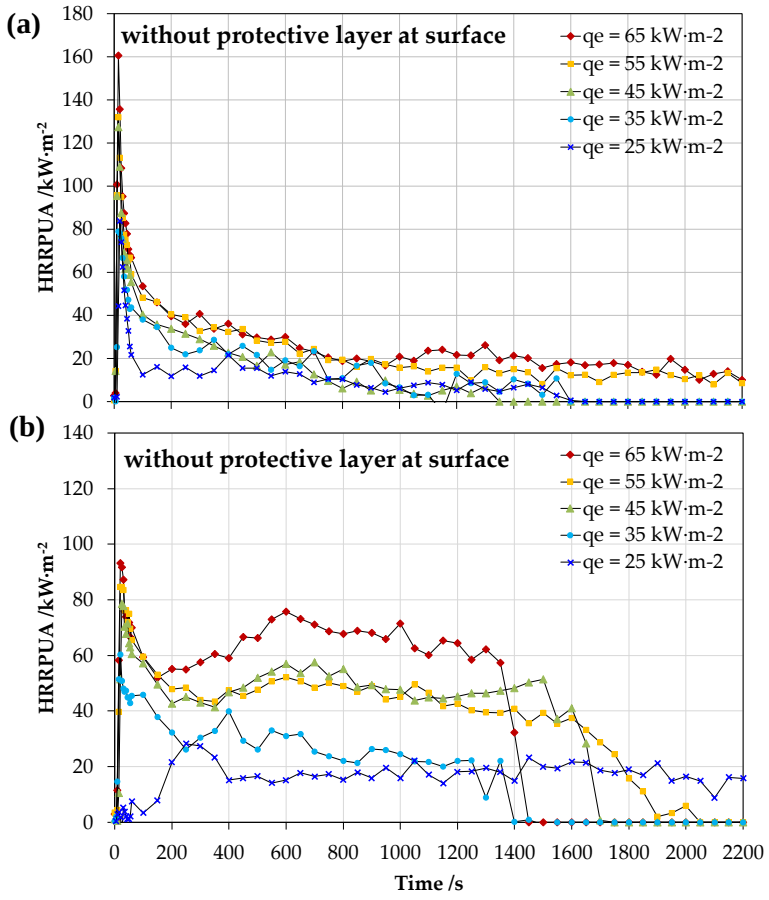

Figure 5. Heat release rate per unit area of 100 mm thick (a) PIRa and (b) PF samples without protective layer at different external heat fluxes. Average from two repetitions.

Table 2 shows the calculated values for the effective heat of combustion for plastic foams PIRa, PIRb, PIRc, and PF. In general, it is observed that the heat of combustion obtained for the pyrolysis gases (flaming) is lower than the effective value obtained considering the total test time.

Table 2. Calculated effective heat of combustion for plastic foams with no protective layer.

Effective Heat of Combustion / kJ·g^{-1}				
Integration time	**PIRa**	**PIRb**	**PIRc**	**PF**
Total test time (t_{end})	19.09 ± 1.99	18.05 ± 2.48	20.52 ± 3.45	20.98 ± 6.01
Up to 200 s (initial flaming)	14.38 ± 0.68	13.22 ± 1.30	16.26 ± 0.84	15.35 ± 0.80

4.1.4. Gas species correlations and yields

Figure 6 shows a selection of gas species correlations of specific tests from PIRa and PF, where high heat fluxes are selected to represent clearly the different phenomena taking place. The charts on the left indicate the CO_2 and CO concentrations, while those on the right indicate the ratio of generated CO_2 versus consumed O_2, and the ratio of generated CO versus CO_2.

For PIR and PF, the CO/CO_2 ratio tended to increase greatly during the progress of the test, suggesting a transition from flaming to smouldering combustion, with both phenomena occurring simultaneously during some periods of the test. A ratio between 0.05 and 0.10 is observed during flaming combustion (time before 200 s) for PIR, and between 0.025 and 0.05 for PF; these values are highlighted in Figure 6 and Figure 7, respectively, with a shading. It is difficult to establish a constant value since a steady-state is not clearly observed. A clear transition from flaming to smouldering combustion cannot be identified as local edge effects are present, thus allowing for flaming at the edges while smouldering occurs at the top surface. The ratio CO/CO_2 continues to increase as the pyrolysis rate and flaming combustion decrease.

With regard to the CO_2/O_2 ratio, a short steady-state was initially obtained for PIR, suggesting only flaming combustion from PIR pyrolysates. This continued to decrease during the period of the test indicating the transition to a different burning regime, probably with char being consumed by oxidation and fewer pyrolysis gases being produced due to the spread of the pyrolysis front through thickness. Similar results were obtained for PF, despite the decrease occurring much earlier, followed by a transition to a quasi-steady-state. This might be indicative of oxidation of char and flaming of pyrolysis gases occurring simultaneously. At the final stage of the test, this was reduced again, probably mainly due to the oxidation of char.

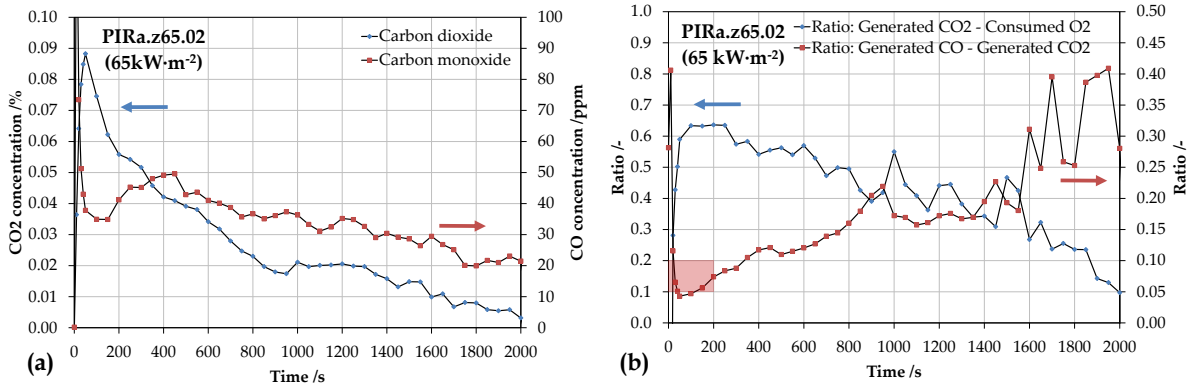

Figure 6. (a) CO_2 and CO concentrations and (b) ratios of generated CO_2 vs consumed O_2 and generated O_2 vs generated CO for PIRa at 65 kW·m^{-2}. The shading denotes the ratio of CO/CO_2 during flaming.

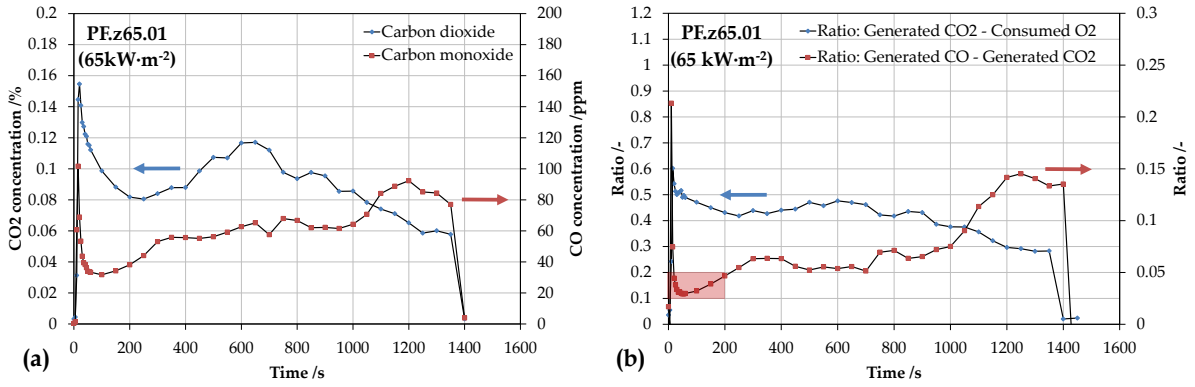

Figure 7. (a) CO_2 and CO concentrations and (b) ratios of generated CO_2 vs consumed O_2 and generated O_2 vs generated CO for PF at 65 kW·m^{-2}. The shading denotes the ratio of CO/CO_2 during flaming.

4.2. Thermal degradation mapping

4.2.1. Isocyanurate-based polyurethane foam (PIR)

Figure 8 shows the time history of the in-depth temperature profile for PIRa experiments tested at 10 kW·m^{-2} with (Figure 8a) and without (Figure 8b) the protective layer at the surface. The in-depth temperature profile is presented for a series of time steps during the test (i.e. from 0 to 10 min using a time step of 2.5 min, and from 10 to 30 min using a time step of 5 min). Vertical error bars show the standard deviation from two repetitions for each thermocouple position. Horizontal error bars indicate the estimated error in the thermocouple positioning. The results from experiments shown in Figure 8a show good repeatability, while those presented in Figure 8b show worse repeatability, especially for temperature measurements near the surface. This is attributed to the non-uniform thermocouple positioning for repeated experiments, which has a larger impact for measurements near the surface potentially due to the swelling of the material during the thermal decomposition process.

Figure 8a shows a case study where no thermal degradation was observed. Positions close to the surface achieved a quasi-steady temperature in early stages (from 2.5 min), with a maximum value of 123 °C ± 4 °C. The temperature profile achieved a quasi-steady state after 20-25 min, with a minimal rate of temperature increase (<1 °C·min^{-1}) for inner positions. The displacement of the thermal gradient towards higher temperatures for inner positions and with steady temperature at the surface is due to the back-boundary layer. The metallic plate, which acts as a heat sink, was slowly increasing in temperature because the thermal wave had reached the sample back face and, consequently, heat was transferred to the plate. The sample section in Figure 8a2 shows that no discolouration was produced in the foam and, consistently, no release of volatiles was observed during the tests.

Figure 8b presents a case study where thermal degradation was observed at the surface of the sample. Thermal gradients were significantly larger than those shown in Figure 8a1, indicating the clear effect of the protective layer on the thermal performance. Positions close to the surface achieved a quasi-steady temperature after 5 min, with a maximum value of 323 °C ± 20 °C, while the temperature profile again achieved a quasi-steady state after 20 min, with a minimal rate of temperature increase (<1 °C·min^{-1}) for inner positions. Three clear tonalities in the discolouration experienced by the sample can be observed in the sample section in Figure 8b2. The discolouration is non-uniform, with higher degradation for regions near the centre-line than near the edge. This indicates that the heat transfer was not behaving perfectly in a one-dimensional regime. Some cracking can be observed near the surface, where the discolouration is darker. Additionally, the sample thickness increased by up to 10 mm. A significant release of volatiles was observed after 3-4 min, but with no ignition during the experiment. Measurements of CO_2 and CO did not present noticeable concentrations compared to the initial baseline; therefore, these are not presented, which confirms that no significant oxidation was produced.

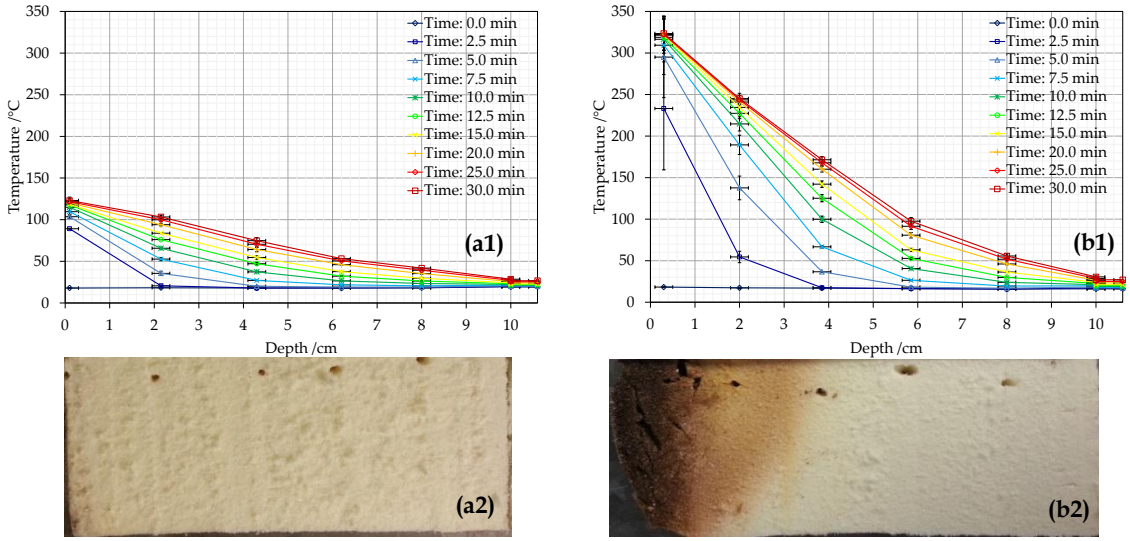

Figure 8. In-depth thermal profiles of PIRa at 10 kW·m^{-2} (a1) with and (b1) without protective layer. Centre-section for the end of the tests (a2, b2).
Horizontal error bars: estimated error of ± 2 mm in thermocouple positioning.
Vertical error bars: standard deviation between two repeated tests.

Figure 9 shows the in-depth temperature profiles for PIRa experiments tested at 25 kW·m^{-2} with (Figure 9a) and without (Figure 9b) the protective layer at the surface. The results from experiments shown in Figure 9a show good repeatability, with vertical error bars being noticeable only for the surface thermocouple. The results from experiments shown in Figure 9b, however, present worse repeatability with the error bars being significantly larger for the three first thermocouples. This non-uniformity is attributed to the positioning and, more importantly, to the degradation processes forming cracks within the sample

and likely different rate of surface oxidation. Significant differences were observed between the performance of the samples with and without the protective layer, which are attributed to the effect that the protective layer has on the radiation absorption due to its low emissivity, and the blocking of air from contact with the surface, thus reducing or cancelling the surface oxidation for those conditions of heating exposure.

Figure 9a presents a case study where small thermal degradation was observed. Positions close to the surface achieved a quasi-steady temperature after 2.5-5 min, with a maximum value of 252 °C ± 5 °C, while the temperature gradient achieved a quasi-steady state after 30 min, with a minimal rate of temperature increase (<0.5 °C·min^{-1}) for inner positions. Two different tonalities can be observed in the sample section shown in Figure 9a2. This indicates that the heat transfer could be considered as a one-dimensional regime. Small cracks can be observed near the surface. Darker tonalities near the edge of the surface, where the foil ends, might be indicative of an edge effect with lower cooling, therefore presenting higher temperatures. Measurements of carbon dioxide and carbon monoxide did not show concentrations displaced from the baseline, confirming that no oxidation occurred. The sample appeared to have slightly expanded by up to 3 mm.

Figure 9b shows a case study where severe thermal degradation was observed. Positions close to the surface achieved a maximum temperature of 591 °C ± 34 °C at 7.5 min. The lack of measurements from the first thermocouple for the subsequent time steps indicates its detachment from the solid due to consumption of the surrounding material. No steady state was observed for the thermal gradient during the final time steps, with the temperature increasing at a rate of 9-10°C·min^{-1} for inner positions. This rapid rate of temperature change indicates the consumption of material at the surface, thus moving the exposed boundary to lower positions. Three to four tonalities can be observed in the sample section shown in Figure 9b2: yellow (virgin material), orange-brown discolouration, and black (char). Small cracks were obtained between the interface of virgin material and orange discolouration, while a series of large cracks can be observed in the brown region, below the char. A thickness regression of approximately 15 mm was obtained, indicating that a significant amount of material was consumed due to surface oxidation.

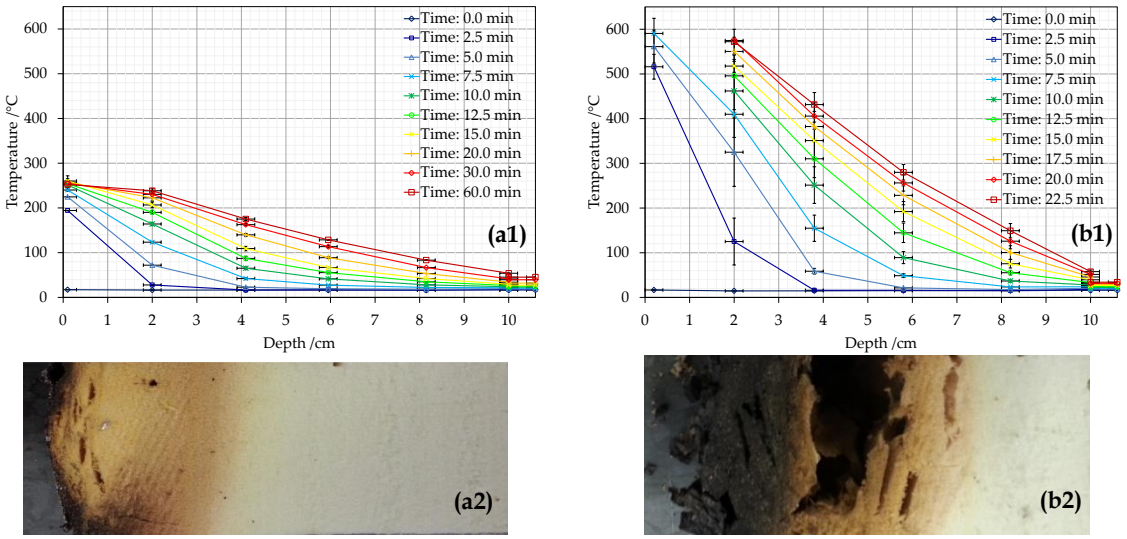

Figure 9. In-depth thermal profiles of PIRa at 25 kW·m^{-2} with (a1) and without protective layer (b1). Centre-section for the end of the tests (a2, b2).
Horizontal error bars: estimated error of ± 2 mm in thermocouple positioning.
Vertical error bars: standard deviation between two repeated tests.

Figure 10 shows the sample residue from different perspectives for the test presented in Figure 9b (25 kW·m^{-2} without protective layer for 22.5 min). The surface of the sample presents complex morphology characterised by craters formed by surface oxidation. It can be observed that the char at the edges and lateral sides of the sample present a smooth morphology, indicating that oxidation did not take place. This is consistent with the set-up that uses aluminium foil to prevent air penetration through the sides, thus limiting oxidation to the top surface.

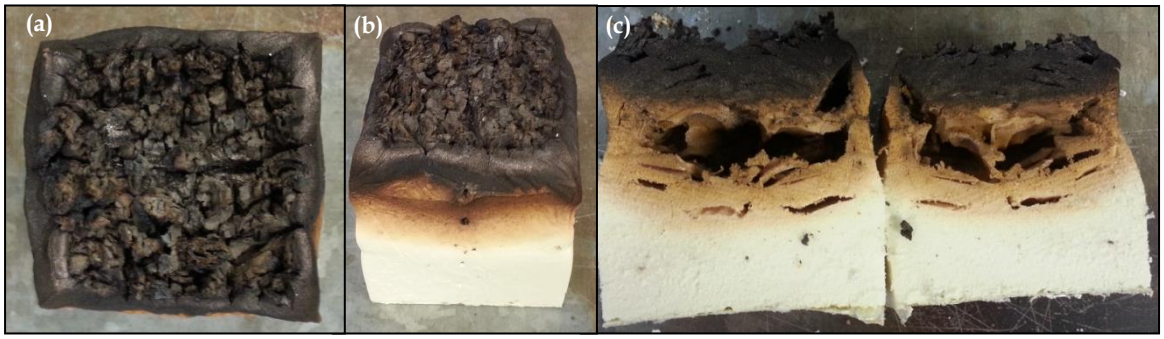

Figure 10. PIRa sample residue at 25 kW·m^{-2} without protective layer up to 22.5 minutes (a) Top view (b) Lateral view (c) Lateral view from section.

A large amount of volatiles were released from the start of the test, shown in Figure 9b and Figure 10, but ignition was not achieved. Despite the fact that the heat flux used was above the critical heat flux, a pilot spark was not used. The release of volatiles continued to decrease after one minute. Measurements of carbon monoxide are presented in Figure 11a with the time-history of temperature measurements. The

concentration of CO increased almost from the beginning, probably indicating generation of pyrolysates. The shape of the CO curve changed slope from 2 to 3 min, and thereafter the CO generation remained approximately under a steady state during the rest of the test. A slight decrease between 10 and 15 min was also observed. These measurements are indicative of smouldering combustion (surface oxidation), with a high CO/CO_2 ratio between 0.8 and 1.2, as shown in Figure 11b. The concentration of CO_2 remained very low in comparison to the generation of CO_2 presented by flaming of PIR pyrolysates in the previous section. Additionally, it is shown that the smouldering was not self-sustained since the thermal gradient and CO generation dropped significantly after the removal of the external heat source. This is due to the closed-cell structure of the foam that does not allow the free circulation of oxygen through the sample, limiting the oxidation to the top surface; therefore, the generation of heat is drastically reduced once the external heat source is removed.

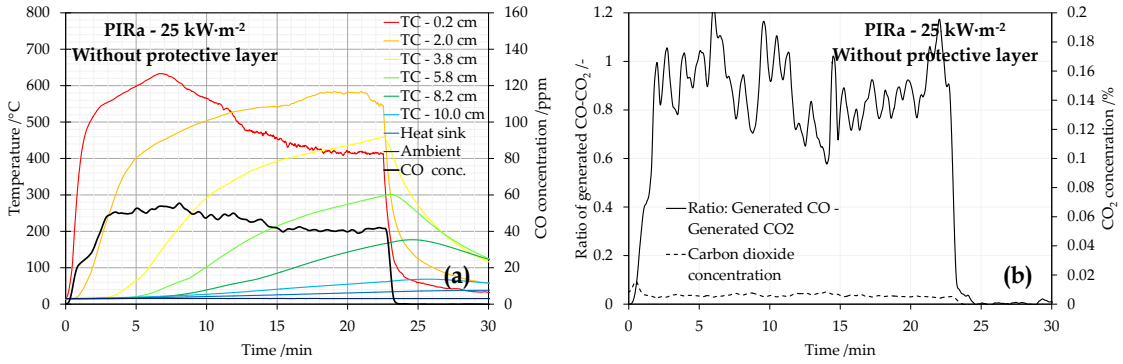

Figure 11. Time-history of temperatures within the solid-phase and CO concentration (a) and generated CO vs generated CO_2 for PIRa with no protective layer at 25 kW·m^{-2}.

A more severe case study is presented in Figure 12, corresponding to a PIRa sample tested at 35 kW·m^{-2} without protective layer. The sample auto-ignited after five seconds of heat exposure, introducing a different regime that was not observed previously for this experimental series, but for the first series studying heat release. Figure 12a shows the time-history of temperatures within the solid-phase and the concentration of generated CO. The thermal evolution within the solid was similar to that presented in Figure 11a, but with a faster heating rate. The generation of CO followed a different pattern due to flaming combustion, which was confirmed by the CO_2 concentration presented in Figure 11b. The CO/CO_2 ratio increased over time, indicating simultaneous flaming and smouldering. This is consistent with the behaviour presented in previous section.

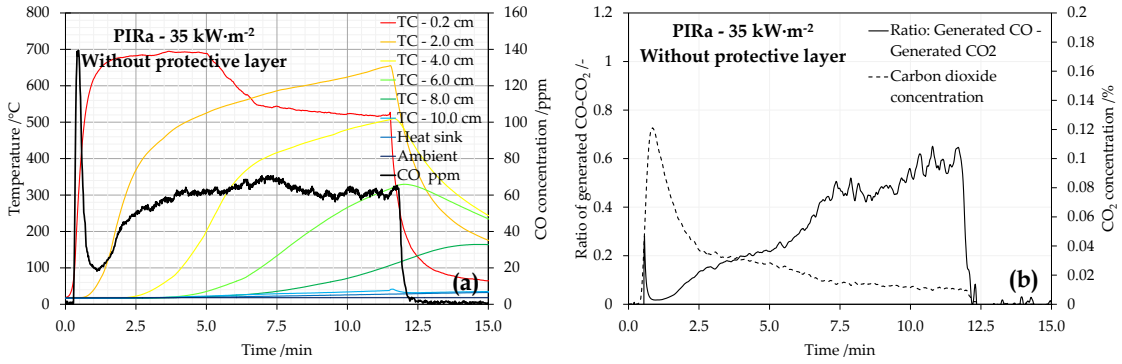

Figure 12. Time-history of temperatures within the solid-phase and CO concentration (a) and generated CO vs generated CO_2 (b) for PIRa with no protective layer at 35 kW·m^{-2}.

The behaviour from PIRb and PIRc foams was similar to the one presented above. The upper edge of the temperature envelopes for PIRa, PIRb, and PIRc at 35 kW·m^{-2} is presented in Figure 13, with a section of the sample after the test. The temperature values were interpolated for the interface between the three main regions of discolouration (yellow, orange-brown and black). In general, the first interface was found between 220°C and 260°C, while the second interface was identified between 460°C and 520°C. The first set of temperatures agrees with the value obtained before the onset of the main peak of pyrolysis observed in differential thermogravimetric (DTG) analyses under nitrogen atmospheres by *Hidalgo et al.* [32, 36]. The second set of temperatures corresponds to the thermal range in which no more significant pyrolysis is obtained under nitrogen atmospheres. Maximum temperatures measured in the solid-phase, presented Figure 13, were near 700°C. Thermogravimetric analyses under air atmospheres (50 ml·min^{-1} flow with 21% of oxygen) showed that the full consumption of mass terminates below 600°C, which indicates that the diffusion of oxygen then dominates the combustion of char at the surface . However, further assessment is required to characterise the mechanisms that govern the combustion of this char.

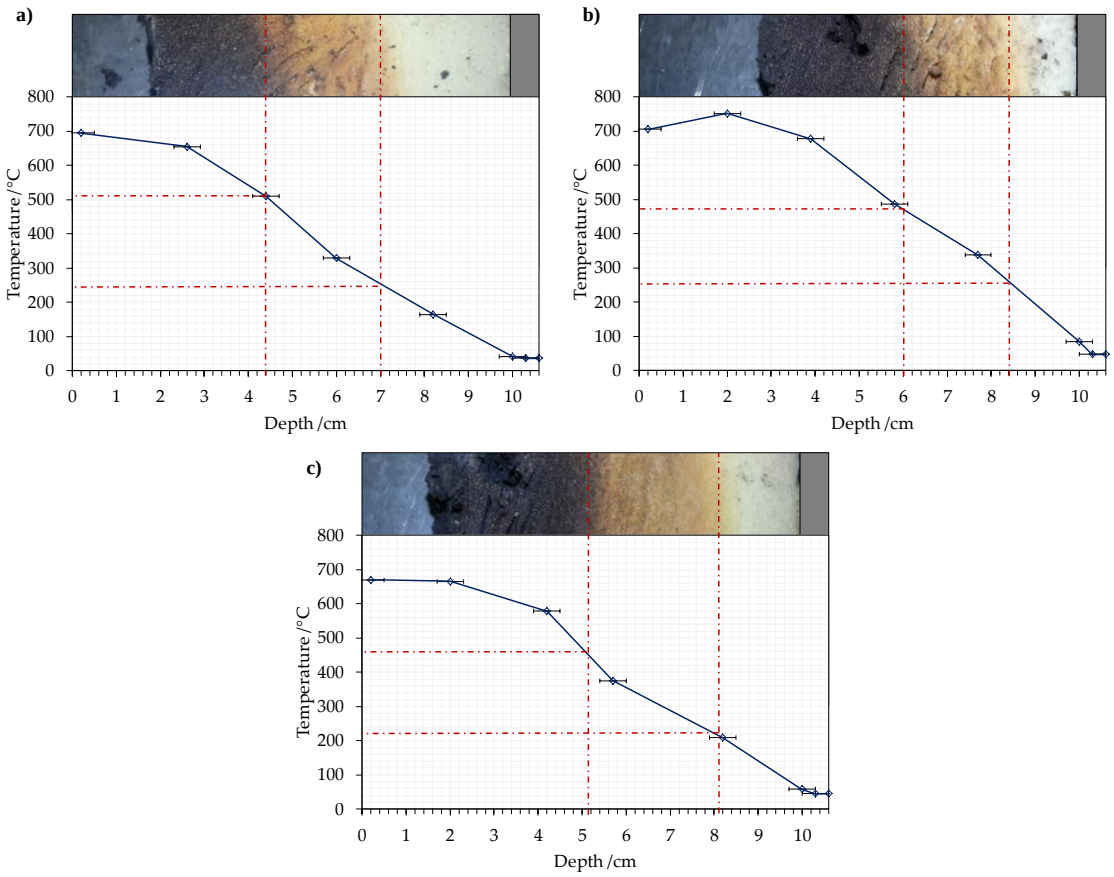

Figure 13. Maximum in-depth temperature profile of (a) PIRa, (b) PIRb and (c) PIRc at 35 kW·m^{-2} (no protective layer). Horizontal error bars: estimated error of ± 2 mm in thermocouple positioning.

4.2.2. Phenolic foam

Figure 14 shows the time history of the in-depth temperature profile for PF experiments tested at 10 kW·m^{-2} with (Figure 14a) and without (Figure 14b) protective layer at the surface. The results from experiments shown in Figure 14a present good repeatability in the experiments, while those from experiments shown in Figure 14b present worse repeatability, especially for temperature measurements obtained by the two first thermocouples. This is attributed to the non-uniformity of the thermocouple positioning and especially to the thermal degradation observed, with char being detached from the surface.

Figure 14a presents a case study where no clear thermal degradation was observed. Positions close to the surface achieved a quasi-steady state from 10 min, with a maximum value of 124 °C ± 1 °C. The temperature profile achieved a quasi-steady state from 15-20 min, with a minimal rate of temperature increase (<1°C·min^{-1}) for inner positions. A change in the slope of the thermal profile was obtained near the second thermocouple once the steady state was achieved. The sample section displayed in Figure 14a2 shows that some discolouration of a darker pink tonality was produced near the surface. Additionally, the

sides and bottom of the section have different tonality than the centre, which indicates that material suffers from oxidation at ambient temperatures. No release of volatiles was observed during the tests.

Figure 14b presents a case study where clear thermal degradation was observed at the surface of the sample. Thermal gradients were significantly larger than the ones shown in Figure 14a, indicating the clear effect of the protective layer on the thermal performance again. The temperature close to the surface achieved a quasi-steady state after 10 min, with a maximum value of 296 °C ± 44 °C at this time step. The temperature profile achieved a quasi-steady state from 25 min, with a minimal rate of temperature increase (<1°C·min^{-1}) for inner positions. The in-depth temperature profile during the steady-state shows an interesting shape, with two different slopes converging at 78 °C, indicating temperature dependency of the thermal properties and/or endothermic processes at lower temperatures. This is consistent with the change of slope observed in Figure 14a. Four clear tonalities in the discolouration experienced by the material can be observed in the sample section shown in Figure 14b2. The degradation seems to be non-uniform, with higher degradation for regions near the centre-line than near the edge. This indicates that the heat transfer was not behaving perfectly as a one-dimensional regime. Cracks and delamination can be observed within the first 20 mm from the surface, in the char area, as shown in Figure 17a. Delamination is probably due to spalling from the sample; popping and snapping sounds could be heard during the experiment. No significant surface regression or oxidation was observed, but measurements of carbon dioxide and carbon monoxide indicated low concentrations compared to the initial baseline. This is indicative of minor oxidation from the delaminated pieces.

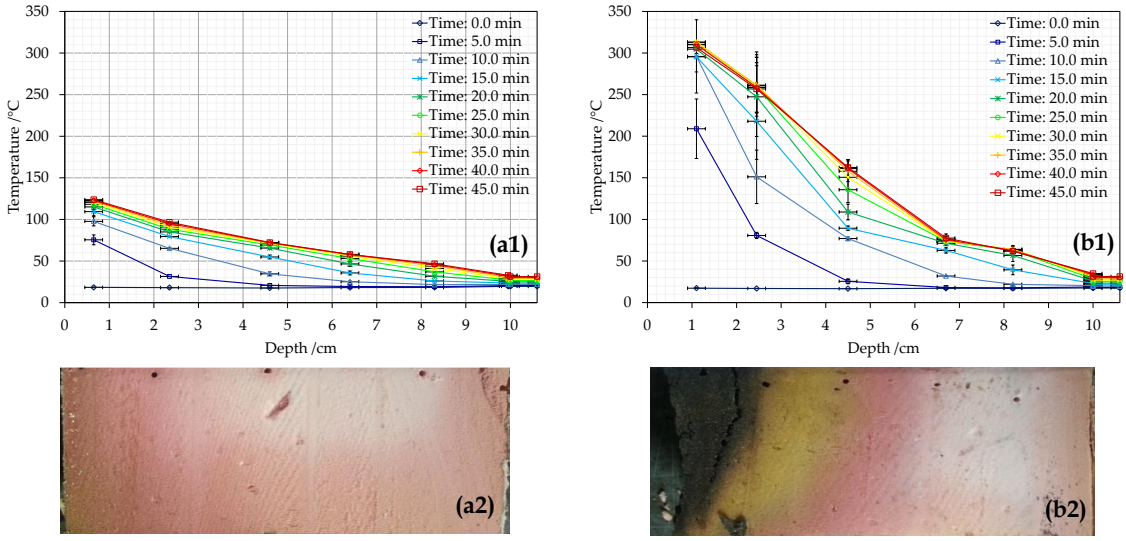

Figure 14. In-depth thermal profiles of PF at 10 kW·m^{-2} with (a1) and without protective layer (b1). Centre-section for the end of the tests (a2, b2).

Horizontal error bars: estimated error of ± 2 mm in thermocouple positioning.
Vertical error bars: standard deviation between two repeated tests.

Figure 15 shows the in-depth temperature profiles for PF experiments tested at 25 $kW \cdot m^{-2}$ with (Figure 15a) and without (Figure 15b) the protective layer at the surface. The results shown in Figure 15a and Figure 15b present good repeatability except for the first thermocouples. Slightly better performance was observed for the samples with a protective layer (Figure 15a) than those without (Figure 15b), with lower thermal gradients for same times of exposure. However, the protective layer did not prevent the onset of thermal degradation.

Figure 15a presents a case study where the effectiveness of the protective layer was lost after certain temperature and thermal degradation was eventually achieved. The temperature profile close to the surface showed a moderate rate of temperature increase around 30-50 $°C \cdot min^{-1}$ until 5 min, achieving a temperature of 204 °C ± 14 °C, at which point the rate of increase rose significantly since the protective layer started to detach and lift after 4 min of heat exposure. As a result, the temperature near the surface achieved a maximum value below 600 °C at around 9 min, when the thermocouple detached from the initial position due to consumption of the surrounding material. Approximately 20 mm of material was consumed by the end of the tests. Four different uniform tonalities can be observed in the sample section between the edge and the centre-line, as shown in Figure 15a2, indicating that the heat transfer could be considered essentially as a one-dimensional regime. No cracks within the core of the sample were obtained, but the top of the sample presented a rough surface with some random cracks. Measurements of carbon dioxide and carbon monoxide showed concentrations displaced from initial baseline, confirming the occurrence of solid-phase oxidation. For simplicity, these results are not presented herein, but for the case shown in Figure 15b which is equivalent.

Figure 15b shows a case study where severe thermal degradation was observed from early times in the test (2.5 min). The temperature close to the surface achieved a maximum value of 592 °C ± 10 °C at 5 min. No steady state was observed for the thermal gradient during the final time steps, with the temperature increasing with a rate of 9-10$°C \cdot min^{-1}$ for inner positions. This rate was only observed for positions with a temperature higher than 100 °C, indicating a clear endothermic effect at that temperature range. A high rate of temperature increase, without achieving the steady-state, indicates the consumption of material at the surface, thus moving the exposed boundary to lower positions. The thermal degradation experienced was similar to that shown in Figure 15a. The surface of the material is presented in Figure 17c, showing crater morphology on the edges and rough surface and random long cracks expanding from the centre to the edges.

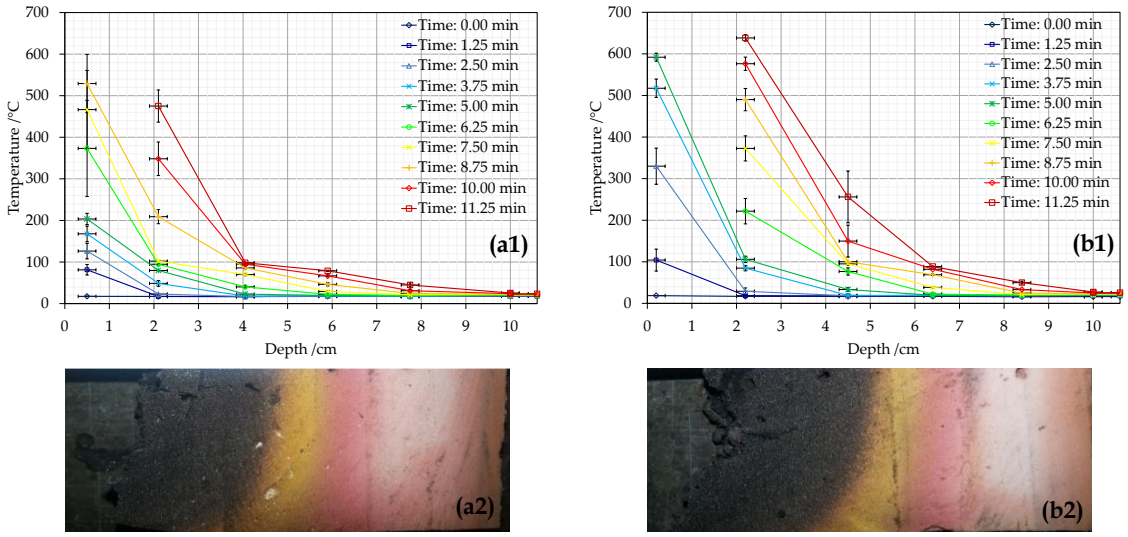

Figure 15. In-depth thermal profiles of PF at 25 kW·m^{-2} with (a1) and without protective layer (b1). Centre-section for the end of the tests (a2, b2).
Horizontal error bars: estimated error of ± 2 mm in thermocouple positioning.
Vertical error bars: standard deviation between two repeated tests.

Measurements of carbon monoxide are presented in Figure 16a with the time-history of temperature measurements. The concentration of CO increased until 5 min, when it achieved a steady state at around 150 ppm. These measurements are indicative of smouldering combustion (surface oxidation), suggesting a constant rate of oxidation. Similarly, the CO/CO_2 ratio increased until 5 min as shown in Figure 16b, remaining approximately constant at around 0.2. The concentration of CO_2 remained very low in comparison to the generation of CO_2 presented for the flaming of PF in previous sections. Additionally, it is shown that the smouldering was not self-sustained since the thermal gradient and CO generation dropped significantly after removing the external heat source. This is due to the closed-cell structure of the foam that does not allow the free circulation of oxygen through the sample. Additionally, a plateau of temperatures was clearly observed below 100°C in Figure 16a, indicating an endothermic reaction, probably due to water desorption in the polymer.

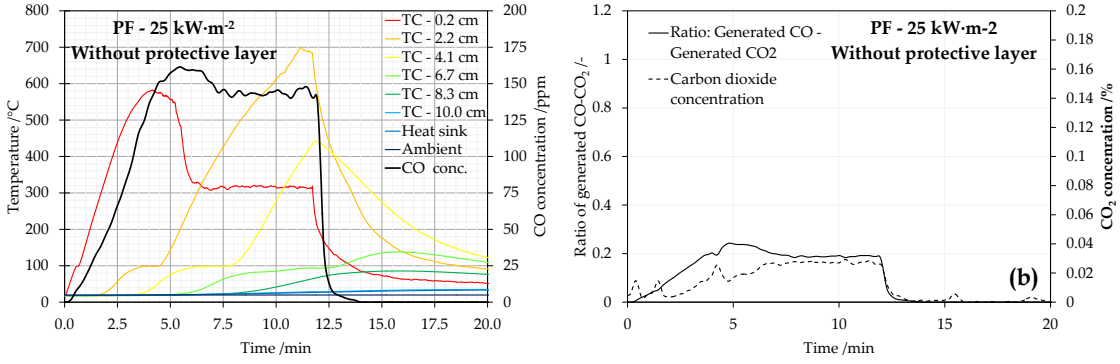

555 Figure 16. Time-history of temperatures within the solid-phase and CO concentration (a) and generated CO
556 vs. generated CO_2 (b) for PF without protective layer at 25 kW·m^{-2}.

557 Images from the surface of the remaining residue for PF experiments without the protective layer at
558 10, 15 and 25 kW·m^{-2} are shown in Figure 17. Different patterns indicate the significance of surface
559 oxidation. Figure 17a shows the occurrence of the delamination effect when the achieved temperatures are
560 not high enough to trigger the oxidation of the char created. Figure 17b shows that the oxidation at the
561 surface is not homogenous, indicating the high complexity of the oxidation mechanism, while Figure 17c
562 shows the case of a smouldering process with relatively constant rate of surface regression as shown in
563 Figure 16.

564 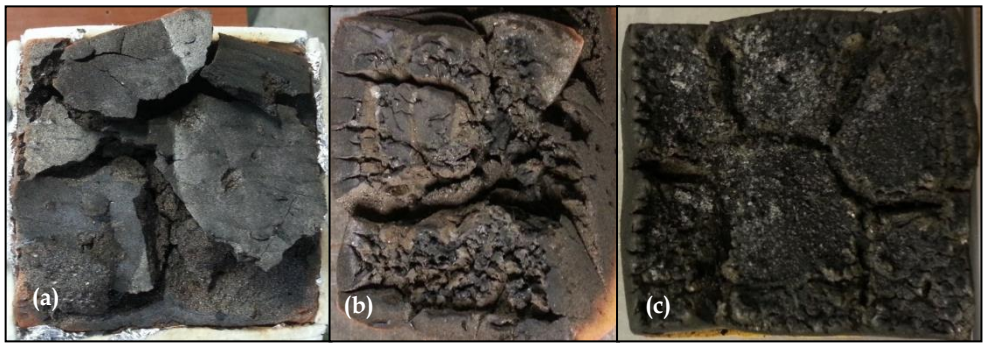

565 Figure 17. PF sample residue at 10 kW·m^{-2} (a), 15 kW·m^{-2} (b) and 25 kW·m^{-2} (c) without protective layer.

566 The upper edge of the temperature envelopes for different experiments are presented separately in
567 Figure 18, together with a section of the sample after the test. Temperatures values were interpolated for
568 the interface between the three main regions of discolouration (light pink, dark pink, orange-brown and
569 black). In general, the first interface, which was observed as a plateau of temperature in Figure 18a, was
570 around 100 °C, near the change of slope in the thermal gradient. The second interface was identified
571 between 125 °C and 160 °C, which agrees with the temperature before the first peak of pyrolysis observed
572 in differential thermogravimetric (DTG) analyses under nitrogen atmospheres in [32, 36]. The third
573 interface was identified between 250 °C and 300 °C, which agrees with the temperature between the first
574 and second peak of pyrolysis observed in DTG analyses under nitrogen atmospheres. Maximum
575 temperatures measured in the solid-phase and shown Figure 18 were between 600 °C and 700 °C, while
576 TGA analyses under air atmospheres showed that all mass consumption ends below 600°C in an air
577 atmosphere. This indicates that the diffusion of oxygen probably dominates the combustion of char at the
578 surface.

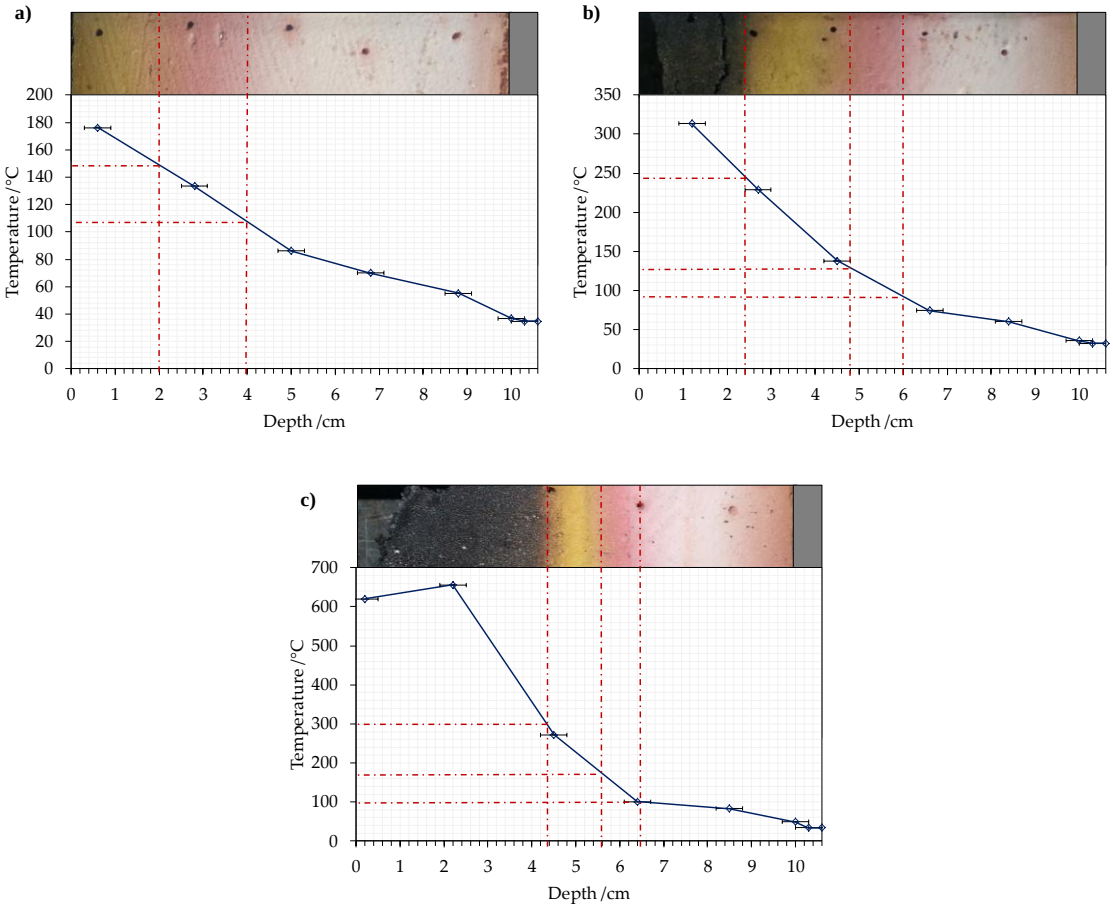

Figure 18. Maximum in-depth temperature profile of PF: a) 15 kW·m^{-2} (foil) b) 10 kW·m^{-2} (no foil) c) 25 kW·m^{-2} (no foil) Horizontal error bars: estimated error of ± 2 mm in thermocouple positioning.

5. Summary

This paper has presented the results from two experimental programmes based on ad-hoc Cone Calorimeter tests. This work aimed to investigate the fire performance of charring closed-cell polymeric insulation materials, specifically polyisocyanurate (PIR) and phenolic foam (PF), so that a comprehensive protocol can be set for assessing the evolution of hazard imposed by the material. The first experimental programme macroscopically analysed the fire performance of these foams by studying heat release rate, mass loss and gas species. The second programme mapped the thermal degradation processes in relation to temperature measurements within the solid-phase, correlating the evolution of the thermal profile experienced by the material to previous results obtained by thermogravimetry.

The first series of experiments was based on 100 mm thick samples tested using the Cone Calorimeter (with spark igniter) and reproducing levels of irradiation from the critical heat flux up to 65 kW·m^{-2}. Calorimetry calculations for PIR and PF samples showed the typical shape obtained from charring materials. A peak of heat release rate per unit area (HRRPUA) between 120-170 kW·m^{-2} was observed for

PIR, with a decay below 60 $kW \cdot m^{-2}$ represented by the formation of a char layer and the transition of the pyrolysis front towards inner depths. The peak heat release rate per unit area for PF was observed to be in the range 80-140 $kW \cdot m^{-2}$, with a decay and subsequent increase or decrease depending on the external heat flux. Despite its larger critical heat flux for ignition, PF showed larger mass loss and surface regression for the same conditions of heat exposure after a certain time. This is attributed to the overlapping of pyrolysis and char oxidation reactions in a close temperature range for PF, while PIR presents clearly separated temperature ranges for the pyrolysis and char oxidation reactions. The effective heat of combustion for PIR was found to be in the range of 13-21 $kJ \cdot g^{-1}$, while for PF the range was 15-21 $kJ \cdot g^{-1}$. Complimentary gas analyses demonstrated different regimes of combustion for PIR and PF, i.e. flaming at the surface with a CO/CO_2 ratio between 0.05 and 0.10 for PIR, and between 0.025 and 0.05 for PF, followed in both cases by smouldering of the char left at the surface, with intermittent flaming at sides and an increasing CO/CO_2 ratio as flaming was reduced. These phenomena may occur simultaneously, depending on the displacement speed of the pyrolysis front and the oxidation rate at the surface.

The second series of experiments was primarily concerned with understanding the thermal evolution and dynamics of the thermal degradation experienced by PIR and PF. This stage was based on 100 mm thick samples tested with the Cone Calorimeter (without spark igniter), and reproducing heating scenarios with different severities. Measurements of temperature within the insulation allowed mapping of the different thermal degradation processes, which were previously identified by thermogravimetric techniques. Measurements of gas species (carbon monoxide, carbon dioxide and oxygen) were also taken to determine whether oxidation processes occurred, i.e. flaming from the pyrolysis gases or smouldering from the char generated after pyrolysis.

A technique based on comparing the eventual thermal discolouration through the thickness of a sample was correlated to the upper edge of the temperature envelopes during the test and the thermogravimetric results. Three clear domains were observed in the thermal evolution of PIR and PF, corresponding to the virgin material, pyrolysis region, and char. Polyisocyanurate was found to expand in the regions where it was pyrolysing, creating a series of cracks or gaps within the structure of the foam. Phenolic foam, however, spalled, probably due to the loss of chemically bound water, which was evidenced by plateaus of temperature around 100°C. A clear effect was observed in the thermal performance of the rigid foams such as PIR and PF when samples were tested with the protective layer attached to the exposed surface. This is related to the reduction of the fraction of absorbed heat flux due to the low emissivity of the protective layer, as well as other effects such as the reduction in the rate of oxidation, via avoiding the contact of oxygen with the charred material or the inhibition of a good mixing between air and pyrolysates.

While the pyrolysis was clearly governed by the thermal evolution of the solid-phase for these charring materials, the rate of oxidation was identified as a diffusion-controlled mechanism. Indeed, values of temperature higher than those obtained by thermogravimetry under air conditions were observed within the char. The rate of oxidation of the char was also found to be governed by the external heat flux, which also determined the evolution of the pyrolysis front. The smouldering process of the char remaining after pyrolysis from PIR and PF was found to self-extinguish after the external heat source was removed. This indicates that the generated heat from the char oxidation at the surface, with the particular heat losses obtained for the tested conditions, was not sufficient to sustain the process. Additionally, the closed-cell structure does not allow the diffusion of air through the foam, thus limiting the smouldering.

Further work should focus on modelling tasks to characterise the thermal behaviour and pyrolysis of these materials. Additionally, the mechanism of char oxidation should be further investigated.

Acknowledgements

The authors would like to gratefully acknowledge funding contribution from Rockwool International A/S towards sponsoring the Ph.D. studies for Juan P. Hidalgo. Michal Krajcovic and Alastair Bartlett are gratefully acknowledged for their precious lab assistance on the performed experimental programmes.

References

1. A.M. Papadopoulos, *State of the art in thermal insulation materials and aims for future developments*, Energy and Buildings, vol. 37, no. 1, pp. 77–86, doi:10.1016/j.enbuild.2004.05.006, 2005.
2. A. Fangareggi, and L. Bertucelli, *Thermoset insulation materials in appliances, buildings and other applications* in Thermosets: Structure, Properties and Applications, pp. 254-288, doi:10.1533/9780857097637.2.254, 2012.
3. EU. *Directive 2010/31/EU of the European Parliament and of the Council of 19 May 2010 on the energy performance of buildings*, Official Journal of the European Union, pp. 13–35, doi:10.3000/17252555.L_2010.153.eng, 2010.
4. U. Krause, W. Grosshandler, and L. Gritzo, *The International FORUM of Fire Research Directors: A position paper on sustainability and fire safety*, Fire Safety Journal, vol. 49, pp. 79-81, doi:10.1016/j.firesaf.2012.01.003, 2012.
5. B. Meacham, B. Poole, J. Echeverria, and R. Cheng, *Fire Safety Challenges of Green Buildings*, Springer New York, doi:10.1007/978-1-4614-8142-3, 2012.

6. J.M. Buist, S.J. Grayson, and W.D Woolley, *Fire and Cellular Polymers*, doi:10.1007/978-94-009-3443-6, 1987.

7. C. Dick, E. Dominguez-Rosado, B. Eling, J.J. Liggat, C.I. Lindsay, S.C. Martin, M.H. Mohammed, G. Seeley, and C.E. Snape, *The flammability of urethane-modified polyisocyanurates and its relationship to thermal degradation chemistry*, Polymer, vol. 42(3), pp. 913-923, doi:10.1016/s0032-3861(00)00470-5, 2001.

8. E. Dominguez-Rosado, J.J. Liggat, C.E. Snape, B. Eling, and J. Pitchel, *Thermal degradation of urethane modified polyisocianurate foams based on aliphatic and aromatic polyester polyol*, Polymer Degradation and Stability, vol. 78(1), pp.1-5, doi:10.1016/S0141-3910(02)00086-1, 2002.

9. I. Vitkauskienė, R. Makuška, U. Stirna, and U. Cabulis, *Thermal Properties of Polyurethane-Polyisocyanurate Foams Based on Poly (ethylene terephthalate) Waste*, Materials Science, vol. 17(3), doi:10.5755/j01.ms.17.3.588, 2011.

10. T.R. Hull, and B.K. Kandola, *Retardancy of Polymers: New Strategies and Mechanisms*, doi: 10.1039/9781847559210, 2009.

11. A.A. Stec, and T.R. Hull, *Assessment of the fire toxicity of building insulation materials*, Energy and Buildings, vol. 43, no. 2-3, pp. 498-506, doi: doi:10.1016/j.enbuild.2010.10.015, 2011.

12. M. Smolka, and Y. Suurenbroek, *Smoke and heat emissions as measures for interaction of tested elements with test environment in fire resistance testing* in Proceedings of the 13th International Interflam Conference, 2013.

13. K.T. Paul, *Burning characteristics of materials*, Fire and Materials, vol. 3(4), pp. 223-231, doi:10.1002/fam.810030408, 1979.

14. K.T. Paul, *Characterization of the burning behaviour of polymeric materials*, Fire and Materials, vol. 8(3), pp. 137-147, doi:10.1002/fam.810080304, 1984.

15. J.M. Buist, S.J. Grayson, and W.D. Woolley, *Fire and Cellular Polymers*, doi:10.1007/978-94-009-3443-6, 1987.

16. M.J. Scudamore, P.J. Briggs, and F.H. Prager, *Cone calorimetry – a review of tests carried out on plastics for the association of plastic manufacturers in Europe*, Fire and Materials, vol. 15(2), pp. 65-84, doi:10.1002/fam.810150205, 1991.

17. T.G. Cleary, and J.G. Quintiere, *NISTIR 4664. Flammability Characterization of Foam Plastics*, National Institute of Standards and Technology, 1991.

18. M. Modesti, A. Lorenzetti, F. Simioni, and M. Checchin, *Influence of different flame retardants on fire behaviour of modified PIR/PUR polymers*, Polymer Degradation and Stability, vol.74(3), pp. 475-479, doi:10.1016/S0141-3910(01)00171-9, 2001.

19. A. Tewarson, and R.F. Pion, *Flammability of plastics—I. Burning intensity*, Combustion and Flame, vol. 26, pp. 85-103, doi:10.1016/0010-2180(76)90059-6, 1976.

20. M. Modesti, and A. Lotenzetti, *Improvement on fire behaviour of water blown PIR–PUR foams: use of an halogen-free flame retardant*, European Polymer Journal, vol.39(2), pp. 263-268, doi:10.1016/S0014-3057(02)00198-2, 2003.

21. A.P. Mouritz, and A.G. Gibson, *Fire Properties of Polymer Composite Materials*, Springer, 2006

22. M.L. Auad, L. Zhao, H. Shen, S.R. Nutt, and U. Sorathia, *Flammability properties and mechanical performance of epoxy modified phenolic foams*, Journal of Applied Polymer Science, vol. 105(3), pp. 1399-1407, doi: 10.1002/app.24405, 2007.

23. W.D. Woolley, *Are Foams a Fire Hazard?* in Fire and cellular polymers, pp. 61–75, doi:10.1007/978-94-009-3443-6_3, 1986.

24. D. Drysdale, *Fundamentals of the fire behaviour of cellular polymers*, Fire and Cellular Polymers, pp. 61-75, doi:10.1007/978-94-009-3443-6_4, 1986.

25. P. J. Briggs, *Fire Behaviour of Rigid Foam Insulation Boards* in Fire and cellular polymers, pp. 117–133, doi:10.1007/978-94-009-3443-6_8, 1986.

26. V. Brannigan, *The regulation of technological innovation: the special problem of fire safety standards*, FireSeat "Fire & Building Safety in the Single European Market", pp. 20-33

27. ASTM D2863. Measuring the minimum oxygen concentration to support candle-like combustion of plastics (oxygen index), ASTM International, West Conshohocken, PA, 2013.

28. BS ISO 5660-1. Reaction-to-fire tests. Heat release, smoke production and mass loss rate. Heat release rate (cone calorimeter method) and smoke production rate (dynamic measurement), BSI, 2015.

29. ASTM E1321. *Standard Test Method for Determining Material Ignition and Flame Spread Properties*, ASTM International, West Conshohocken, PA, 2013.

30. J.P. Hidalgo, S. Welch, and J.L. Torero, *Performance criteria for the fire safe use of thermal insulation in buildings*, Construction and Building Materials, vol. 100, pp. 285-297, doi:10.1016/j.conbuildmat.2015.10.014, 2015.

31. J.P. Hidalgo, S. Welch, and J.L. Torero, *Design tool for the definition of thermal barriers for combustible insulation materials*, Proceedings of the 2nd IAFSS European Symposium of Fire Safety Science, ISBN 978-9963-2177-0-0, 2015.

32. J.P. Hidalgo, J.L. Torero, and S. Welch, *Experimental characterisation of the fire behaviour of thermal insulation materials for a performance-based design methodology*, Fire Technology (in press), doi:10.1007/s10694-016-0625-z, 2017.

33. J.P. Hidalgo, N. Gerasimov, R.M. Hadden, J.L. Torero, and S. Welch, *Methodology for estimating pyrolysis rates of charring insulation materials using experimental temperature measurements*, Journal of Building Engineering, vol. 8, pp. 249-259, doi: 10.1016/j.jobe.2016.09.007, 2016.

34. BS EN 13501-1. Fire classification of construction products and building elements. Part 1: Classification using data from reaction to fire tests, 2009.

35. BS EN 1363-1. Fire resistance tests - Part 1: General Requirements, 2012.

36. J.P. Hidalgo, *Performance-Based Methodology for the Fire Safe Design of Insulation Materials in Energy Efficient Buildings*, Ph.D. Thesis, The University of Edinburgh, http://hdl.handle.net/1842/10601, 2015.

37. S. Quinn, *Chemical blowing agents: providing production, economic and physical improvements to a wide range of polymers*, Plastics, Additives and Compounding, vol. 3. pp. 16–21, doi:10.1016/S1464-391X(01)80162-8, 2001.

38. R. Carvel, T. Steinhaus, G. Rein, and J.L. Torero, *Determination of the flammability properties of polymeric materials: A novel method*, Polymer Degradation and Stability, vol. 96, no. 3, pp. 314–319, doi:10.1016/j.polymdegradstab.2010.08.010, 2011.

39. J. V. Beck, *Thermocouple Temperature Disturbances in Low Conductivity Materials*, Journal of Heat Transfer, vol. 84, no. 2, pp. 124, doi:10.1115/1.3684310, 1962.

40. P. Reszka, *In-Depth Temperature Profiles in Pyrolyzing Wood*, Ph.D. thesis, The University of Edinburgh, http://hdl.handle.net/1842/2602, 2008.

41. W.M. Thornton, *The relation of oxygen to the heat of combustion of organic compounds*, Philosophical Magazine Series, vol. 33, pp. 196–203, 1917.

42. A. Tewarson, *Generation of Heat and Chemical Compounds in Fires*, in SFPE Handbook of Fire Protection Engineering, 3rd ed., P.J. DiNenno, D. Drysdale, C.L. Beyler, W.D. Walton, R.L.P. Custer, and J.M. Watts, Eds. Massachusetts, U.S.A.: National Fire Protection Association, 2002.

43. M.L. Janssens, *Measuring rate of heat release by oxygen consumption*, Fire Technology, vol. 27, no. 3, pp. 234–249, doi:10.1007/BF01038449, 1991.

44. H. Biteau, T. Steinhaus, C. Schemel, A. Simeoni, G. Marlair, N. Bal, and J. Torero, *Calculation Methods for the Heat Release Rate of Materials of Unknown Composition*, Fire Safety Science, vol. 9, pp. 1165–1176, doi:10.3801/IAFSS.FSS.9-1165, 2008.